J. Chem. Sci. (2019)131:93
https://doi.org/10.1007/s12039-019-1665-y

REGULAR ARTICLE

Special Issue on Materials Chemistry

Influence of ionic liquids and concentration of red phosphorous on luminescent Cu_3P nanocrystals

YOGENDRA NATH CHOURYAL, RAHUL KUMAR SHARMA, DEBOPAM ACHARJEE, TRISIT GANGULY, ARCHNA PANDEY and PUSHPAL GHOSH*

Department of Chemistry, School of Chemical Science and Technology, Dr. Harisingh Gour University (A Central University), Sagar 470 003, Madhya Pradesh, India
E-mail: pushpalghosh27@gmail.com

MS received 31 March 2019; revised 9 May 2019; accepted 15 May 2019

Abstract. Highly crystalline, phase pure Cu_3P nanocrystals (NCs) have been successfully synthesized using ionic liquid-assisted solvothermal method at relatively low temperature (200 °C). Herein, ionic liquids (ILs) are used as a structure directing/templating agent. Effect of ILs and precursor concentration on crystal phase, crystallite size, lattice strain, morphology and grain size of Cu_3P NCs is studied. In the presence of IL, crystallite size and lattice strain significantly change with changing the concentration of red phosphorus. For example, smaller crystallite size (38.5 nm) and compressive lattice strain are obtained when 10 times of red phosphorous is used. However, bigger size (41.9 nm) and tensile lattice strains are obtained for the lower concentration of phosphorous (5 times). At higher phosphorus concentration, hexagonal shaped micro-crystals with prominent grain are observed. HRTEM images reveal that spherical-shaped particles on further agglomeration through Ostwald ripening process form hexagonal-shaped bigger microstructures. However, on doping the rare-earth ions ($RE^{3+} = Ce^{3+}/Tb^{3+}$) in the Cu_3P NCs show the green luminescence (at 542 nm) which is attributed to the emission of Tb^{3+} ions. To the best of our knowledge, this is the first report on rare-earth doped Cu_3P nanoparticles and shows promise on the luminescence aspect of Cu_3P nanomaterials along with its already existing plasmonic and semiconducting properties.

Keywords. Nanocrystals; rare-earth; copper phosphide; photoluminescence; ionic liquids.

1. Introduction

Recently nanocrystalline transition metal phosphides have been emerged as a promising class of semiconducting nanomaterials for numerous applications.[1–18] For instance, CoP, NiP and FeP nanoparticles have been employed as a electrocatalyst for hydrogen evolution and lithium ion storage.[3,4] However, CdP, InP and Zn_3P_2 nanoparticles have shown prominent optical properties leading to numerous optical applications such as photovoltaic, telecommunication and so on.[5–10] Amongst those, copper phosphide (Cu_3P) is selected due to various reasons which make it a promising candidate for optoelectronic applications due to having both the plasmonic and semiconducting properties. Copper is a very cheap element, non-toxic and has high natural abundance. In addition, Cu_3P has dual properties; it can be used in high efficiency catalysis and also exhibits plasmonic property.[19–22] As a result, it is extensively employed for various applications including superconductivity, potential in magnetic recording media, anode materials in lithium ion battery, showing good electrochemical performances, light emitting, photovoltaic, oxygen reduction reaction, carbon dioxide reduction, methanol/ethanol oxidation, water splitting and so on.[2,12–18] Cu_3P NCs are P-type semiconducting nanomaterials with band gap of about 1.3–1.6 eV. Judicious choice or fabrication of synthesis protocols is utmost important to control the size of Cu_3P NCs which will control the size dependent optical properties.[19–21] Many researchers have synthesized Cu_3P NPs at high

*For correspondence

Electronic supplementary material: The online version of this article (https://doi.org/10.1007/s12039-019-1665-y) contains supplementary material, which is available to authorized users.

Published online: 03 October 2019

temperature using several methods. For examples, mechanochemical, solvothermal reactions, co-reaction using organometallic reagents with phosphines are employed which leads to different types of structural and optical properties.[11,22–25] Most of the researchers have used P_2S_5, yellow/red/white phosphorus, tricotyl phosphine (TOP) and phosphine gas as a phosphorous precursor.[19–25]

Doping of transition metal or rare-earth (RE^{3+}) ions in semiconducting nanomaterials is very interesting to obtain nanomaterials with desired properties including optical, photocatalytic activity, etc.[26–29] There are numerous semiconducting nanomaterials like ZnS, In_2S_3, GaN, etc. which have been used as host matrix for doping of RE^{3+} ions (Er^{3+}, Ce^{3+}, Eu^{3+}, etc.) for getting luminescent nanomaterials for various applications.[26–29] Interestingly, excitation and emission spectra of RE^{3+} doped luminescent nanomaterials are independent of size of host matrix due to confined 4f–4f intraconfigurational transitions which are highly shielded by 5s and 5p orbitals.[30–32] Till now, the literature related to RE^{3+} doped Cu_3P NCs is not reported to the best of our knowledge. Cu_3P nanomaterials show semiconducting as well as plasmonic property.[19] However, judicious doping of RE^{3+} ions in Cu_3P NCs would increase its applications in visible region of solar spectra.

Normally, for the preparation of nanoparticles and tuning their crystal phase, morphology and band gap, amine-based capping/templating agents are being employed which have drastic impact on the environment.[33–38] In this context, it has become an obligation to develop the environmentally benign synthesis protocols to design the nanoparticles with desired functions. So, IL-assisted synthesis of nanoparticles is getting tremendous attention.[33–38] ILs usually possess organic/inorganic cation and inorganic anion moieties and having melting point below 100 °C in ambient conditions. By varying the alkyl chain length of cation, nature of cation (aromatic or non-aromatic) and anion, changing the cation–anion combination, concentration and viscosity, the physicochemical properties of ILs can be tuned which will further tune the structural and optical properties of nanomaterials.[34–36] Thus, ILs are considered as a "*green and designer solvent*". In many cases, ILs are not only being employed as a capping/templating agent, solvent but also can be used as a reaction partner too.[11,33,34,38]

Herein, we have successfully synthesized Cu_3P NCs using IL-assisted solvothermal method. Thereafter, influence of ILs and red phosphorus concentration on the crystal phase, lattice strain, and morphology of Cu_3P NCs is studied. It is noticed that crystallite size is decreasing with phosphorus concentration in the presence of 1-ethyl-3-methylimidazolium bromide ($[C_2mim]Br$) IL. Lattice strain changes from tensile to compressive with increasing phosphorus concentration. Substantial effect of ILs is found on the morphology and grain boundary of Cu_3P NCs. It is noticed that in case of ally-based IL, grain boundary is not so much prominent and surface is smoother than that of other ILs. Furthermore, on doping of Ce^{3+}/Tb^{3+} ions in Cu_3P NCs, emission is obtained in green region.

2. Experimental

2.1 *Chemicals*

Cuprous chloride [CuCl] (LobaChemie, 99.9%), Red phosphorous [P] (LobaChemie, 99.9%), 1-methylimidazolium [$C_4H_6N_2$] (Alfa Aesar, 99%), 1,2-dimethyl imidazole [$C_5H_8N_2$] (Sigma Aldrich 99%), Bromoethane [C_2H_5Br] (Himedia, 99%), Bromobutane [C_4H_9Br] (Himedia, 99%), Allyl bromide [C_3H_5Br] (Himedia, 99%), Tetramethyl ammonium bromide [$(CH_3)_4NBr$] (TMAB) (Himedia, 99%), Ethyl acetate [$C_2H_5COOCH_3$] (LobaChemie, 99%) Acetone [C_3H_6O], (LobaChemie, 99.5%), Diethyl ether [$(C_2H_5)_2O$] (LobaChemie, 99%), Deionized water [H_2O] (CDH).

2.1a *1-ethyl-3-methyl imidazolium bromide [C_2mim]Br*: Modifying a literature procedure, 1-ethyl-3-methylimidazolium bromide [C_2mim]Br is synthesized by incorporation of 12.4 mL bromoethane [C_2H_5Br], and 10 mL N-methyimidazole [$C_4H_6N_2$] and refluxed in a round bottom flask (250 mL) at 40 °C for 4 h in an inert gas (Ar) atmosphere. After the completion of reaction, the obtained product was washed with ethyl acetate [$C_4H_8O_2$] and stirred for 1 h. Then it was filtered and dried in vacuum for 12 h to get a white solid.[39]

2.1b *1-Ethyl- 1,2-dimethylimidazolium bromide [C_2 dmim]Br*: Modifying a literature procedure, 1, 2-dimethyl-imidazolium, [C_2dmim]Br is synthesized by mixing of 53.82 mL of 1,2-dimethyl imidazole, and 58.91 mL of bromoethane and then refluxed in a round bottom flask (250 mL) under inert atmosphere at 40 °C for 3 h. After the completion of reaction, the obtained product was washed with ethyl acetate and stirred for 1 h. Then it was filtered and dried in vacuum for 12 h to get a white solid.[40]

2.1c *1-Allyl-3-methylimidazolium bromide [Amim]Br*: Modifying a literature procedure, 1-allyl-3-methylimidazolium bromide [$C_7H_{11}BrN_2$] is synthesized by mixing N-methyimidazole [$C_4H_6N_2$] and allyl bromide [C_3H_5Br], and then refluxed in a round bottom flask (250 mL) under inert atmosphere at 40 °C for 3 h. After the completion of reaction, the obtained product was washed with ethyl

acetate and stirred for 1 h. Then it was filtered and dried in vacuum for 12 h to get a white solid.[40]

2.2 *Synthesis of Cu_3P NCs*

First judicious amount of ILs (for example, 0.5 g [C_2mim]Br), Cuprous chloride (0.669 g) and Red phosphorous (0.0698 g) are mixed with deionized water. Then the solution is stirred at room temperature for 5 min and the mixture was poured into a Teflon lined autoclave and heated at 200 °C for 14 h. When the autoclave was cooled to room temperature in ambient condition, the black product was centrifuged (2000 rpm for 10 min) and was washed with water and diethyl ether to remove the other impurities. And the final black product was dried in a hot air oven for 12 h.

2.3 *Synthesis of doped Cu_3P:Ce^{3+}/Tb^{3+} NCs*

Here we have synthesized Cu_3P:Ce^{3+}/Tb^{3+} NCs using the above-mentioned method for undoped Cu_3P NCs. Here only Cerium nitrate (0.0099 g) and Terbium nitrate (0.0100 g) are mixed along with Copper and Phosphorus precursors. Thereafter, as-obtained particles are washed using the same procedure.

2.4 *Characterizations*

PXRD was carried out on a D8 Advance BRUKER, equipped with Cu-Kα (1.54060 Å) as the incident radiation. The crystallite size was calculated using Scherer equation $D = K\lambda/\beta\cos\theta$, where D represents crystallite size (Å), K= 0.9, λ is the wavelength of Cu-Kα radiation and β is the corrected half width of the diffraction peak. Morphological characterization was also carried out by SEM using a NOVA NANO SEM-450, FEI. TEM (FEI Tecnai STWIN-T30 using 200 kV electron beam source) was used to map the shape, size and lattice structure of the NCs dispersed on a carbon-coated copper grid from acetone solution. Photoluminescence emission and excitation spectra were measured through HORIBA JOBIN YVON made Fluoromax-4 spectrofluorometer.

3. Result and Discussion

3.1 *Structural analysis using PXRD*

3.1a *Effect of reaction temperature and reaction time*: First different synthesis parameters like reaction temperature and reaction time are tuned to optimize the synthesis for Cu_3P nanoparticles (Figure 1). Here, the concentration of phosphorous is taken 5 times more than its stoichiometric

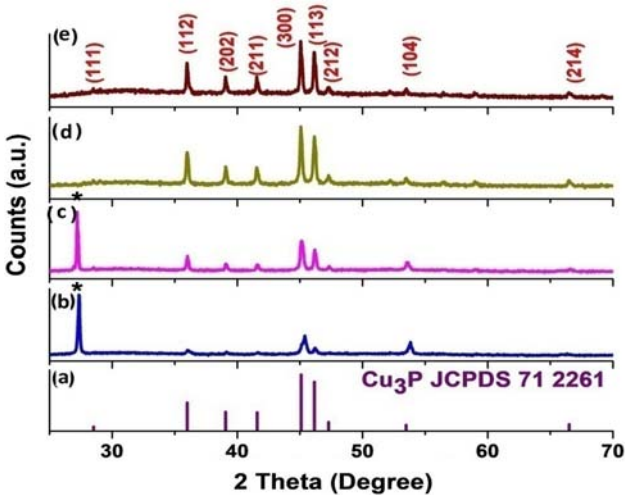

Figure 1. PXRD patterns of Cu_3P NCs: (**a**) Standard Cu_3P, (**b**) prepared in presence of [C_2mim]Br, at 150 °C for 24 h reaction time; (**c**) prepared in presence of [C_2mim]Br, at 200 °C for 9 h reaction time; (d) prepared without IL at 200 °C for 14 h, and (e) prepared in presence of [C_2mim]Br, at 200 °C for 14 h reaction time. All are prepared using 5 times phosphorus.

concentration in all cases. When the synthesis is performed at 150 °C for 24 h in the presence of [C_2mim]Br IL, there is no formation of phase pure Cu_3P NCs (Figure 1b). Impurity at lower angle (2θ = 27.23) is observed due to presence of unreacted cuprous chloride (shown by asterisk *). This indicates that the reaction is not completed at 150 °C. Thereafter, reaction temperature is increased to 200 °C and reaction time is gradually increased to 9, 14 and 24 h. Similar impurity of unreacted cuprous chloride (shown by asterisk *) is observed for the synthesis occured at 200 °C for 9 h (Figure 1c). Phase pure Cu_3P NCs are obtained from 14 h reaction time at 200 °C (Figure 1d, e). All peaks are nicely matching with JCPDS card no. 71-2261. For the remaining reactions, reaction temperature and time are set to 200 °C and 14 h respectively (shown in Table 1). No change in crystal phase of NCs is noticed. However, crystallite size is considerably changed. For example, bigger crystallite size (ca. 49.9 nm) is obtained in absence of IL in comparision to that of NCs (41.9 nm) which are synthesized using IL ([C_2mim]Br), under similar experimental conditions (Figure 1d, e and Table 1). This clearly indiactes that IL is working as a capping agent or templating agent in the nanoparticle synthesis.

3.1b *Effect of phosphorous concentration*: Like reaction temperature and reaction time, concentration of phosphorous has also significant effect in

Table 1. Cu_3P NCs, their reaction time, reaction temperature, phosphorous concentration, particle size and their lattice strain.

Sample code*	Ionic liquid (IL 1%)	Reaction time (h)	Reaction temperature (°C)	Conc. (P)*	Particle size (nm)	Lattice strain (%)	Tensile/compressive
CP1	NO	14	200	5P	49.9	9.22	Tensile
CP2	[C_2mim]Br	14	200	5P	41.9	5.95	Tensile
CP3	[C_2mim]Br	14	200	10P	38.5	− 3.02	Compressive
CP4	[Amim]Br	14	200	5P	49.3	6.72	Tensile
CP5	TMAB	14	200	5P	45.8	6.88	Tensile
CP6	[C_2dmim]Br	14	200	5P	45.1	7.59	Tensile

*CP = Cu_3P, P = phosphorous concentration.

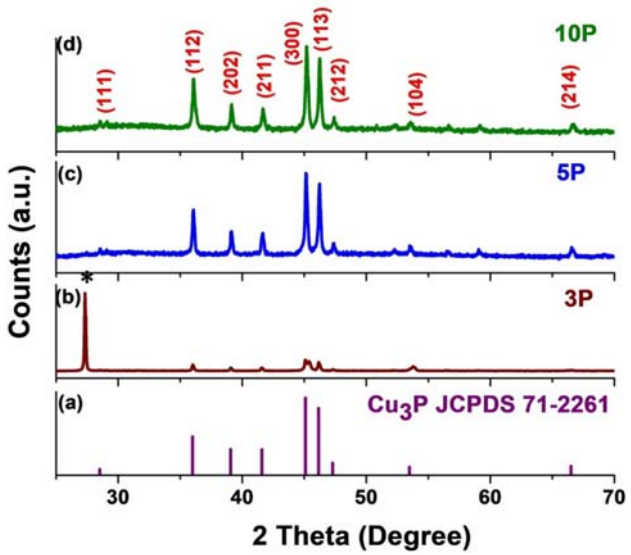

Figure 2. PXRD patterns of Cu_3P NCs: (**a**) Standard Cu_3P JCPDS Card, (**b**) prepared with 3 times phosphorus concentration at 200 °C for 24 h, (**c**) prepared with 5 times phosphorus concentration at 200 °C with 14 h, and (**d**) prepared with 10 times phosphorus concentration at 200 °C for 14 h. In all cases [C_2mim]Br IL is used.

nanoparticle formation (Figure 2). No phase pure Cu_3P nanoparticles are formed till 3 times phosphorus concentration (Figure 2b). In this case, unreacted CuCl is obtained as impurity which is indicated by asterisk (*). However phase pure Cu_3P nanoparticles with cubic phase are observed when 5 times phosphorous is used at 200 °C and with 14 h reaction time (Figure 2c). When phosphorous concentration is increased to 10 times, no change in crystals phase is observed (Figure 2d). However, significant effect on crystallite size of the Cu_3P NCs under the similar conditions is noticed. Crystallite size is gradually decreasing with increasing the phosphorus concentration. For instance, 41.9 and 38.5 nm crystallite size is obtained for 5 and 10 folds red phosphorus concentration respectively under the similar reaction conditions. From this, it is clearly evident that concentration of red phosphorus has significant impact on the purity and crystallite size of as-obtained NCs.

3.1c *Effect of ionic liquids (ILs)*: After studying the influence of phosphorus concentration, role of different ionic liquids (ILs) such as [C_2mim]Br, [C_2dmim]Br, [Amim]Br, and TMAB are studied (Figure 3). Here, we have tuned ILs by substituting the acidic proton situated at C-2 position, alkyl group at C-1 position (ethyl, allyl) and taking IL with non-aromatic system (tetramethylammonium ion). Then it is studied how these influence on the crystal phase, crystallite size of the Cu_3P NCs. It is noticed that the

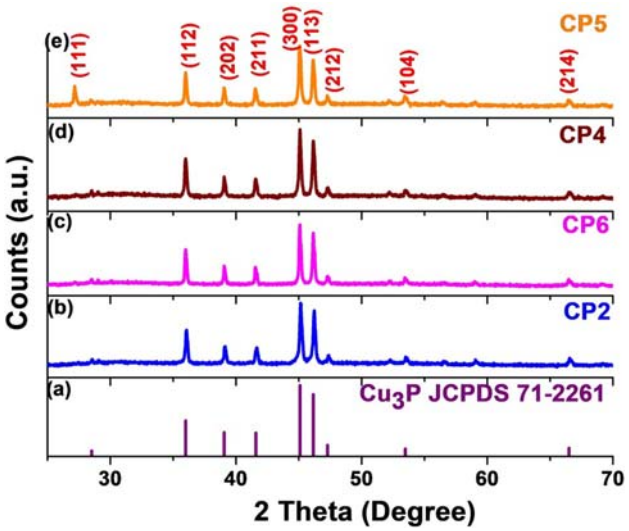

Figure 3. PXRD patterns of Cu_3P NCs: (**a**) Standard Cu_3P JCPDS Card, (**b**) prepared in presence of [C_2mim]Br, (**c**) prepared in presence of [C_2dmim]Br, (**d**) prepared in presence of [Amim]Br and (**e**) prepared in presence of TMAB. All are synthesized using 5 times phosphorus and in the presence of different ILs (1%) at 200 °C and 14 h.

crystal phase is same in all the cases. But there is a change in the crystallite size. For example, when [C_2mim]Br is used, 41.9 nm is noticed for the crystallite size. Here it can be anticipated that binding to the nanoparticle site can occur through aromatic π system or H bonding. To confirm this, we have used [C_2dmim]Br where H at C-2 position is replaced by a methyl group and crystallite size is noticed increasing (45.1 nm). So it gives a clear indication that along with aromatic π system, hydrogen bonding is also playing an important role.

When [Amim]Br is used (Figure 3d), 49.3 nm is observed for crystallite size which is bigger than the [C_2mim]Br. This clearly indicates that due to bigger size allyl group in C-1 position, IL cation facing steric hindrance compared to [C_2mim]Br analogue. Similarly 45.8 nm crystallite size is obtained when IL with non-aromatic system like TMAB is used (Figure 3e). Our study confirms that binding of ionic liquids at the nucleation site of Cu_3P is very important to obtain nanoparticles of desired crystallite site.

3.2 *Lattice strain*

Normally, lattice strain varies with changing the crystallite size of NCs. This can be rationalized using the Williamson-Hall equation which can be expressed as:

$$\beta \cos\theta/\lambda = 1/D + \eta \sin\theta/\lambda \quad (1)$$

where β is the full width at half-maximum (FWHM), θ is the diffraction angle, λ is the X-ray wavelength, D is the effective crystallite size and η is the effective strain. On plotting graph between $\beta\cos\theta/\lambda$ vs sin θ/λ, the lattice strain can be determined from the slope. The positive and negative magnitudes of the slope infer the tensile and compressive strain respectively.

Lattice strain results clearly show that by varying the concentration of red phosphorus, tensile strain is decreasing and then render to compressive strain (-Figure 4a, e). For instance, when 5 times phosphorus concentration is used, tensile strain (5.95%) is found (Figure 4a). On the other hand, on increasing the concentration of phosphorus to 10 folds, lattice strain is changed to compressive strain (−3.02%) [shown in Figure 4e]. These changes can be illustrated on the basis of crystallite size. Interestingly, in the presence of [C_2mim]Br IL, when 10 folds concentration of red phosphorus was employed, smallest crystallite size (i.e. 38.5 nm) is found. In other words, this size can be attributed to critical size of Cu_3P NCs from where compressive strain is observed. Maximum value of tensile strain (9.22%) is obtained for the Cu_3P NCs which are synthesized using no IL (Figure S1, Supplementary Information). However, value of tensile strain is found less for sample which is synthesized using IL than that of sample synthesized without IL. It means, ILs are serving as capping agent. Interestingly, on changing the alkyl chain length, removing acidic proton situated at C-2 position of imidazolium cation and changing the nature of cation from aromatic cation (imidazolium) to non-aromatic (tetramethylammonium) cation of IL, significant influence on lattice strain is observed. Tensile strain gradually increases with changing the ILs (Figure 4a–d).

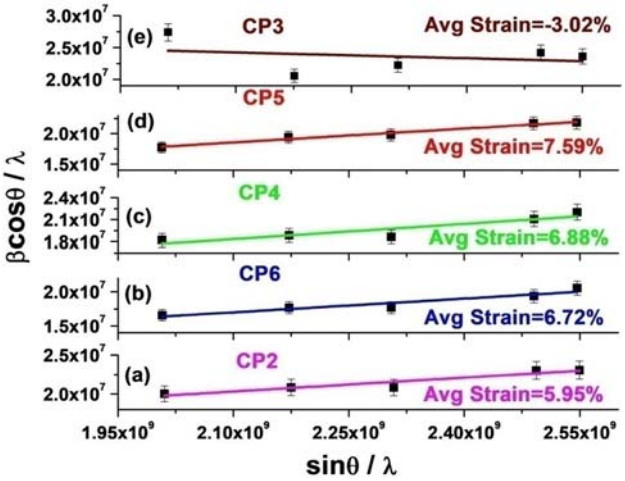

Figure 4. Lattice strain of as-prepared Cu_3P NCs: (**a**) 5 times phosphorus with [C_2mim]Br IL, (**b**) 5 times phosphorus with [C_2dmim]Br IL, (**c**) 5 times phosphorus with [Amim]Br IL, (**d**) 5 times phosphorus with TMAB IL and (**e**) 10 times phosphorus with [C_2mim]Br IL. All are synthesized using (1%) IL at 200 °C for 14 h.

3.3 *Morphology analysis by scanning electron microscopy*

Figure 5 depicts the FESEM images of as-prepared Cu_3P NCs at different concentration of phosphorus and ILs which are synthesized using solvothermal method. These images illustrate that bigger size of particles with prominent grain is occurring in the absence of IL while the particles are comparatively smaller and having less prominent grain boundary in the presence of [C_2mim]Br IL, prepared under the same reaction condition (shown in Figure 5a, b). And morphology of Cu_3P NCs is irregular shaped. However, when the

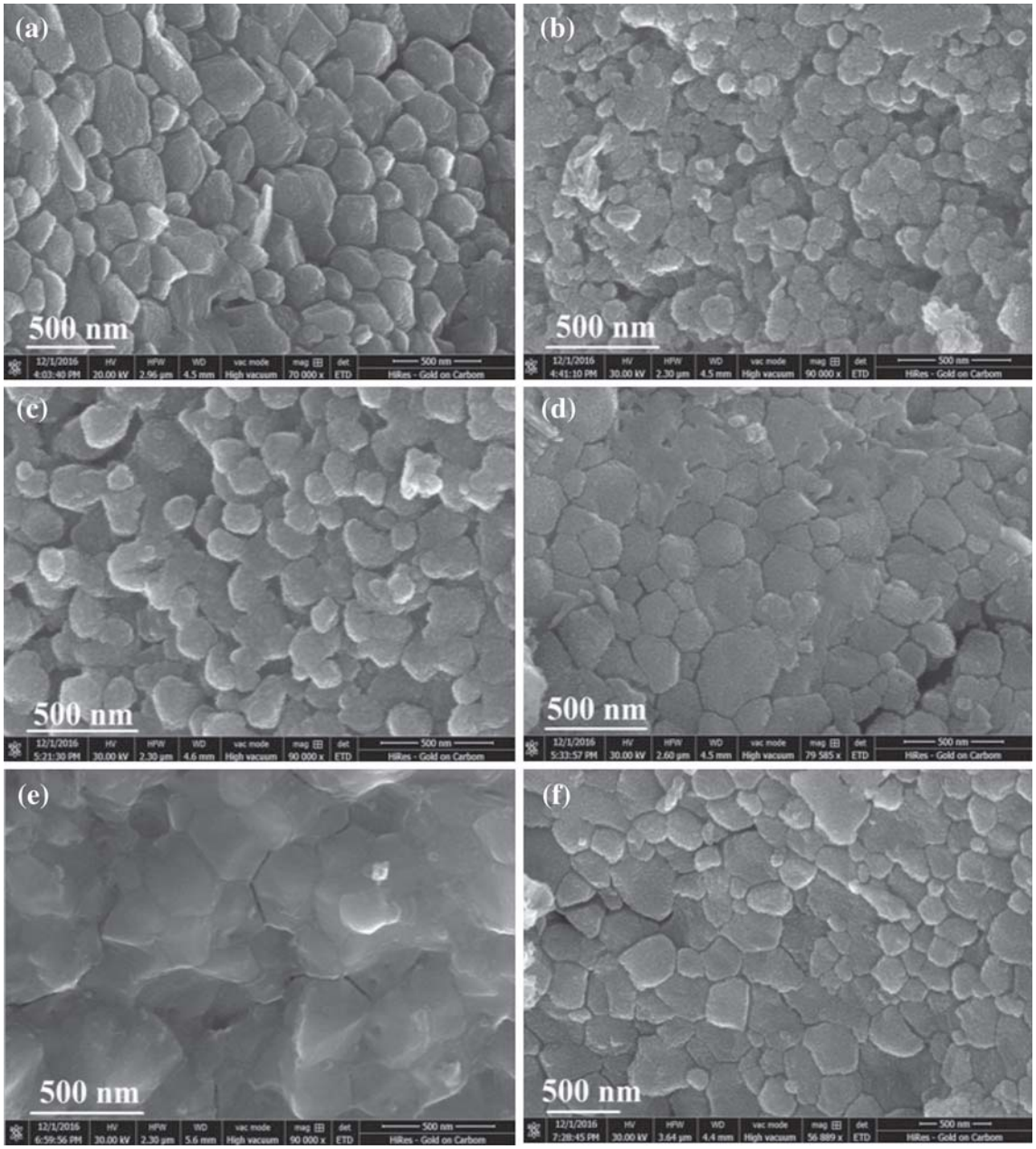

Figure 5. FESEM images of Cu_3P NCs: (**a**) 5 times phosphorus without IL, (**b**) 5 times phosphorus with [C_2mim]Br IL, (**C**) 10 times phosphorus with [C_2mim]Br IL, (**d**) 5 times phosphorus with [C_2dmim]Br, (**e**) 5 times phosphorus with [Amim]Br IL and (**f**) 5 times phosphorus with TMAB IL which are synthesized at 200 °C for 14 h.

concentration of red phosphorus increased to 10 folds, remarkable change in morphology is observed, not only the grain boundary is changing but also shape of Cu_3P NCs is becoming to regular hexagonal-shaped particles (Figure 5c). In other words, hexagonal shape can be further confirmed by finding the numbers of particles present around the centre particle. For instance, each central particle is surrounded with six different particles as can be seen in Figure 5d. It means each particle is coordinated with six different particles resulting in appearance of hexagonal shape. In the case of [Amim]Br, grain boundary is not clear and surface of particles is smoother compared to the particles which are synthesized using other ILs or without IL (shown in Figure 5e and S2E).

From Figure 5f and S2F, it is seen that mainly pentagonal nanoagglomerate is observed when TMAB is used. Above analysis clearly reveals that ILs have a considerable impact on morphology of the as-prepared Cu_3P NCs. High magnification FESEM images of these samples are shown in Figure S2, Supplementary Information.

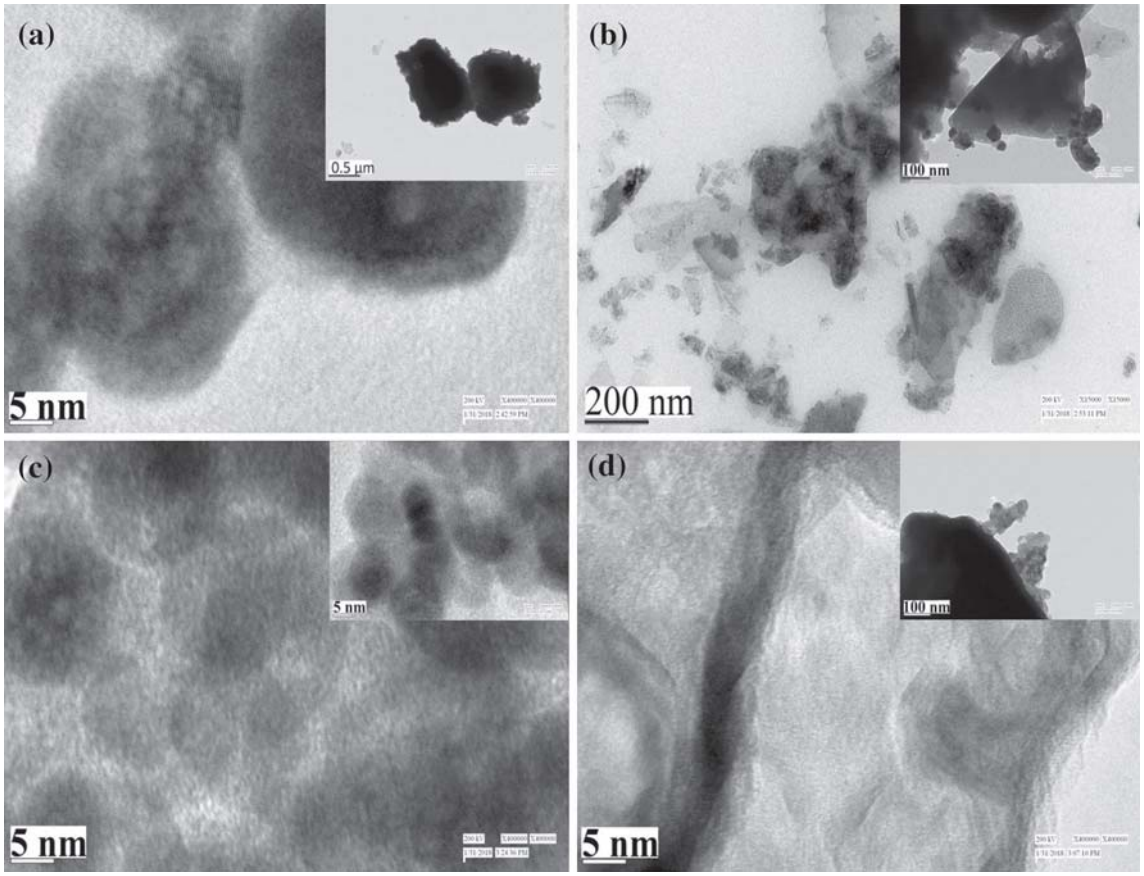

Figure 6. High resolution and low (inset) resolution TEM images of as-prepared Cu_3P NCs: (**a**) without IL, (**b**) with [C_2mim]Br, (**c**) with [Amim]Br and (**d**) with TMAB. All samples are prepared using 5 times phosphorus with different ILs (1%) at 200 °C for 14 h.

3.4 *Morphology analysis by transmission electron microscopy*

To get more insight about the growth of particles at nanoscale, low magnification and HRTEM images are analyzed (Figure 6). These images are basically made up of spherical-shaped particles, which are on further agglomeration through Ostwald ripening leading to form hexagonal-shaped bigger microstructures (Scheme 1).

It has been seen that, particles are more agglomerated in the absence of IL than that of NCs which are prepared in the presence of IL (Scheme 1 and Figure 6a, b). Being spherical and easily disturbed with electron beam during measurement, apparently it was difficult to see lattice fringes. Interestingly, it has been noticed that in the absence and presence of IL except TMAB, particles seem more or less spherical (Figure 6a–c). On the other hand, in presence of TMAB, particles have not prominent shape (Figure 6d). At the same time, spherical nanoparticles are obtained when [Amim]Br is used (Figure 6c). It is clearly noticed that radius of the spherical nanoparticles will be 10–15 nm.

3.5 *Energy Dispersive X-ray analysis (EDX)*

To confirm whether the dopant ions (Ce^{3+} and $Tb^{3+)}$ are properly incorporated in the Cu_3P NCs or not, EDX of as-prepared Ce/Tb co-doped Cu_3P NCs is measured. EDX result clearly shows that Ce^{3+} and Tb^{3+} ions are nicely incorporated in the Cu_3P NCs (Figure 7).

3.6 *Optical property*

Along with pure and undoped Cu_3P NCs, RE^{3+} ions (Ce and Tb) doped Cu_3P NCs are also prepared. Figure 8a, b depict the excitation and emission spectra of Ce/Tb co-doped Cu_3P NCs which are prepared using [C_2mim]Br IL at 200 °C. As-prepared Cu_3P:Ce/Tb NCs are black powder. So there is a significant challenge to get good emission. On exciting the Ce^{3+}-doped Cu_3P NCs at 278 nm, broad emission peak around 340–380 nm appears which corresponds to 5d–4f transition of Ce^{3+} ion (Figure S3 a, b, Supplementary Information).[30,31] Figure 8a shows the

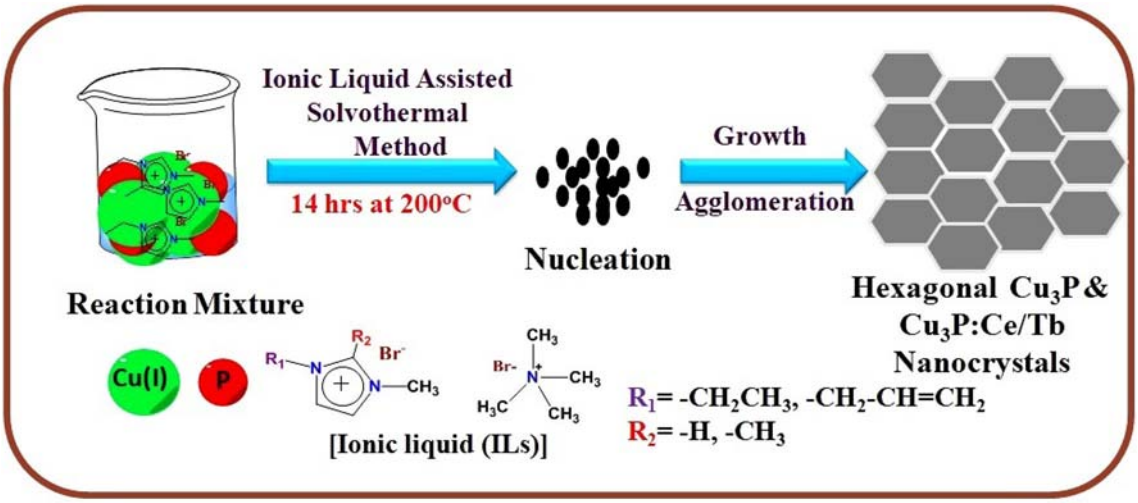

Scheme 1. Schematic representation of synthesis of Cu_3P and Ce/Tb co-doped Cu_3P nanocrystals in presence of ionic liquids.

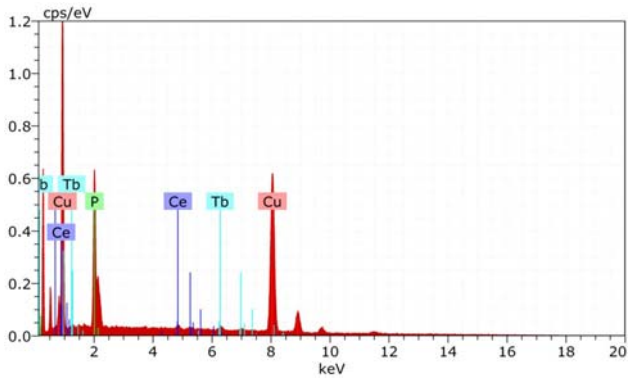

Figure 7. EDX of as-prepared Ce/Tb co-doped Cu_3P NCs synthesized using 5 times phosphorus with $[C_2mim]Br$ IL at 200 °C and 14 h.

excitation spectra of Ce^{3+} and Tb^{3+} co-doped Cu_3P NCs being monitored at 542 nm. Appearance of peak at 278 nm is due to 4f–5d transition.[30,31] On exciting at 278 nm, normally energy transfer is taking place from Ce^{3+} to Tb^{3+} ions.[30,31]

Thereafter, non-radiative decay occurs to the excited level $^5D_4$ of Tb^{3+} ions followed by radiative decay to numerous underlying levels $^7F_{0\text{-}6}$ of Tb^{3+} ions. As a result, characteristic emission peaks of Tb^{3+} ion at 482, 542, 585 and 621 nm correspond to $^5D_4$–$^7F_6$, $^5D_4$–$^7F_5$, $^5D_4$–$^7F_4$ and $^5D_4$–$^7F_3$ transitions, respectively are found in Cu_3P:Ce/Tb NCs (shown in Figure 8b).[30,31] The highly intense green emission is observed at 542 nm ($^5D_4$–$^7F_5$ transition) which is regarded as magnetic dipole transition of J = ±1 (Figure 8b).[30,31]

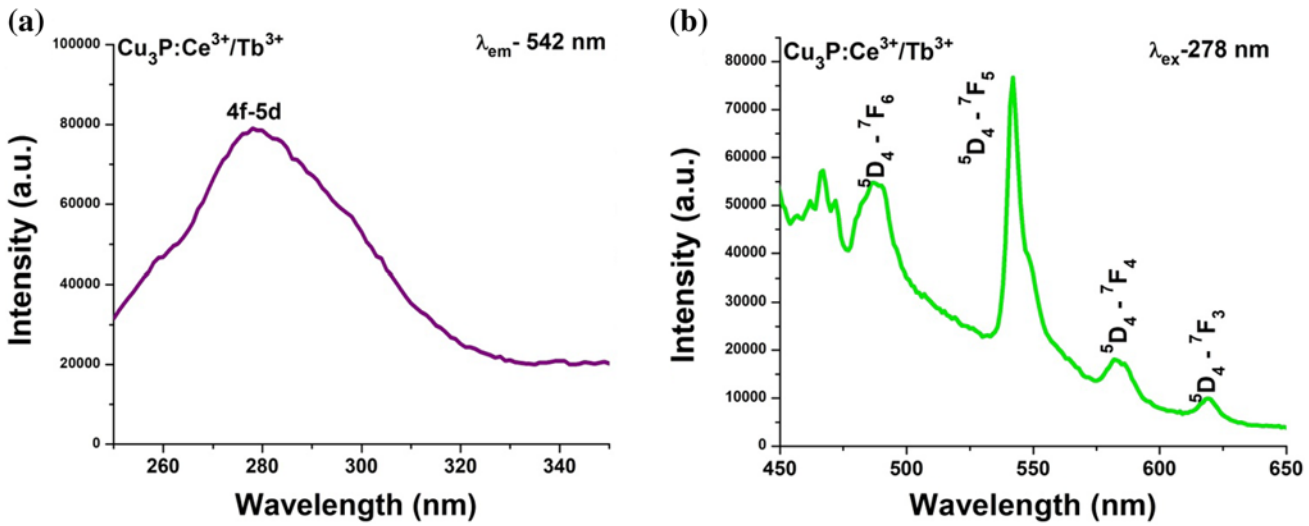

Figure 8. Photoluminescence spectra of as-prepared Ce^{3+} and Tb^{3+} co-doped Cu_3P NCs: (**a**) excitation spectrum [λ_{em} = 542 nm] and (**b**) emission spectrum [λ_{ex} = 278 nm]. This sample is synthesized using 5 times phosphorus with $[C_2mim]Br$ IL at 200 °C for 14 h.

4. Conclusions

In summary, we have successfully synthesized Cu_3P NCs using ILs assisted solvothermal approach. Herein ILs are employed as structure directing agent. Analysis reveals that ILs, reaction temperature, concentration of red phosphorous and reaction time has significant effect on crystallite size, lattice strain and morphology of Cu_3P NCs. Crystallite size is decreased on sequentially increasing the phosphorus concentration. Consequently, lattice strain is also changed from tensile to compressive when high phosphorous concentration is used. However, crystallite size of as-prepared Cu_3P NCs is found less in the presence of ILs compared to the NCs synthesized without IL. In addition, morphology is also significantly changed in the presence of IL and concentration of phosphorus. Shape of Cu_3P NCs gradually changes from spherical to hexagonal or pentagonal-shaped. Furthermore, we have successfully doped the Ce and Ce/Tb ions in Cu_3P NCs which is further confirmed through EDX analysis. As a result, green emission is found on exciting the Ce/Tb-doped Cu_3P NCs. This emission is attributed to energy transfer process which is taking place from Ce^{3+} to Tb^{3+} ion. This result confirms that other rare-earth ions can also be incorporated inside Cu_3P NCs which may enhance the applications aspects of Cu_3P NCs. Along with its interesting semiconducting and plasmonic properties, Cu_3P nanomaterials can be used as luminescent materials also when they are doped with judiciously chosen rare-earth ions. For example, by doping with Er^{3+}/Yb^{3+} ions in Cu_3P host lattice, efficient upconverting materials can be obtained. However by doping with Gd^{3+}/Eu^{3+} ions, quantum cutting materials useful for energy efficient lighting may be obtained. In addition, understanding the band gap and photoluminescence properties of Cu_3P nanomaterials is very much important to explore various important applications.

Supplementary Information (SI)

Lattice strain of Cu_3P NCs synthesized using 5 times phosphorus, without IL and at 200 °C for 14 h (Figure S1). FESEM images of as-prepared Cu_3P NCs: A) 5 times phosphorus without IL, B) 5 times phosphorus with [C_2mim]Br, C) 10 times phosphorus with [C_2mim]Br, D) 5 times phosphorus with [C_2dmim]Br, E) 5 times phosphorus with [Amim]Br, and F) 5 times phosphorus with TMAB which are prepared at 200 °C for 14 h (Figure S2). Photoluminescence spectra of as-prepared Ce doped Cu_3P NCs: (a) excitation measured at λ_{em} = 372 nm and (b) emission at λ_{ex} = 278 nm synthesized using 5 times phosphorus with [C_2mim]Br IL at 200 °C and 14 h (Figure S3, Supplementary Information) are available at www.ias.ac.in/chemsci.

Acknowledgements

The authors would like to acknowledge for financial support from the Science and Engineering Research Board (SERB) and Board of Research in Nuclear Sciences (BRNS), Government of India. The authors acknowledge Sophisticated Instrumentation Centre (SIC) for SEM, and Department of Chemistry for PXRD analysis. The authors also acknowledge the AIIMS New Delhi for TEM characterization support from PURSE programme sanctioned by Department of Science and Technology (DST), Govt of India.

References

1. Callejas J F, Read C G, Roske C W, Lewis N S and Schaak R E 2016 Synthesis, characterization, and properties of metal phosphide catalysts for the hydrogen-evolution reaction *Chem. Mater.* **28** 6017
2. Wei K, Qi K, Jin Z, Cao J, Zheng W, Chen H and Cui X 2016 One-step synthesis of a self-supported copper phosphide nanobush for overall water splitting *ACS Omega* **1** 1367
3. Du H, Kong R-M, Guo X, Qu F and Li J 2018 Recent progress in transition metal phosphides with enhanced electrocatalysis for hydrogen evolution *Nanoscale* **10** 21617
4. Sun M, Liu H, Qu J and Li J 2016 Earth-rich transition metal phosphide for energy conversion and storage *Adv. Energy Mater.* **13** 1600087
5. Miao S, Hickey S G, Rellinghaus B, Waurisch C and Eychmüller A 2010 Synthesis and characterization of cadmium phosphide quantum dots emitting in the visible red to near-infrared *J. Am. Chem. Soc.* **132** 5613
6. Greuters J and Rizvi N 2003 UV laser micromachining of silicon, indium phosphide and lithium niobate for telecommunications applications. In: Thomas J. Glynn (ed.), Proceedings of SPIE Opto-Ireland 2002: Optics and photonics technologies and applications Vol. **4876**
7. Luber E J, Mobarok M H and Buriak J M 2013 Solution-processed zinc phosphide (α-Zn_3P_2) colloidal semiconducting nanocrystals for thin film photovoltaic applications *ACS Nano* **7** 8136
8. Bhushan M and Catalano A 1981 Polycrystalline Zn_3P_2 Schottky barrier solar cells *Appl. Phys. Lett.* **38** 39
9. Bachmann K J 1981 Properties, preparation, and device applications of indium phosphide *Annu. Rev. Mater. Sci.* **11** 441
10. Bera D, Qian L, Tseng T K and Holloway P H 2010 Nanocrystals for thin film photovoltaic applications quantum dots and their multimodal applications: a review *Materials* **3** 2260
11. Wolff A, Pallmann J, Boucher R, Weiz A, Brunner E, Doert T and Ruck M 2016 Resource-efficient high-yield ionothermal synthesis of microcrystalline $Cu_{3-x}P$ *Inorg. Chem.* **55** 8844

12. Hao J, Yang W, Huang Z and Zhang C 2016 Superhydrophilic and superaerophobic copper phosphide microsheets for efficient electrocatalytic hydrogen and oxygen evolution *Adv. Mater. Interfaces* **3** 1600236
13. Shen R, Xie J, Ding Y, Liu S-y, Adamski A, Chen X and Li X 2019 Carbon nanotube-supported Cu_3P as high-efficiency and low-cost cocatalysts for exceptional semiconductor-free photocatalytic H_2 evolution *ACS Sustain. Chem. Eng.* **7** 3243
14. Kong M, Song H and Zhou J 2018 Metal–organophosphine framework-derived N,P-codoped carbon-confined Cu_3P nanopaticles for superb Na-ion storage *Adv. Energy Mater.* **8** 1801489
15. Hua S, Qu D, An L, Jiang W, Wen Y, Wang X and Sun Z 2019 Highly efficient p-type Cu_3P/n-type g-C_3N_4 photocatalyst through Z-scheme charge transfer route *Appl. Catal. B* **240** 253
16. Zheng H, Huang X, Gao H, Lu G, Dong W and Wang G 2019 Cu@Cu_3P Core–shell nanowires attached to nickel foam as high-performance electrocatalysts for the hydrogen evolution reaction *Chem. Eur. J.* **25** 1083
17. Wang R, Dong X-Y, Du J, Zhao J-Y and Zang S-Q 2018 MOF-Derived Bi-functional Cu_3P nanoparticles coated by a N, P-Co-doped carbon shell for hydrogen evolution and oxygen reduction *Adv. Mater.* **30** 1703711
18. Wolff A, Doert T, Hunger J, Kaiser M, Pallmann J, Reinhold R, Yogendra S, Giebeler L, Sichelschmidt J, Schnelle W, Whiteside R, Gunaratne H Q N, Nockemann P, Weigand J J, Brunner E and Ruck M 2018 Low-temperature tailoring of copper-deficient $Cu_{3-x}P$-electric properties, phase transitions, and performance in lithium-ion batteries *Chem. Mater.* **30** 7 111
19. Manna G, Bose R and Pradhan N 2013 Semiconducting and plasmonic copper phosphide platelets *Angew. Chem.* **125** 6894
20. Kristensen A, Yang J K, Bozhevolnyi S I, Link S, Nordlander P, Halas N J and Mortensen N A 2017 Plasmonic colour generation *Nat. Rev. Mater.* **2** 16088
21. De Trizio L, Gaspari R, Bertoni G, Kriegel I, Moretti L, Scotognella F and Marras S 2015 $Cu_{3-x}P$ nanocrystals as a material platform for near-infrared plasmonics and cation exchange reactions *Chem. Mater.* **27** 1120
22. Stan M C, Klöpsch R, Bhaskar A, Li J, Passerini S and Winter M 2013 Cu_3P binary phosphide: synthesis via a wet mechanochemical method and electrochemical behavior as negative electrode material for lithium-ion batteries *Adv. Energy Mater.* **3** 231
23. Barry B M and Gillan E G 2008 Low-temperature solvothermal synthesis of phosphorus-rich transition-metal phosphides *Chem. Mater.* **20** 2618
24. Wang X, Han K, Gao Y, Wan F and Jiang K 2007 Fabrication of novel copper phosphide (Cu_3P) hollow spheres by a simple solvothermal method *J. Cryst. Growth* **307** 126
25. Liu J, Meyns M, Zhang T, Arbiol J, Cabot A and Shavel A 2018 Triphenylphosphite as the phosphorus source for the scalable and cost-effective production of transition metal phosphides *Chem. Mater.* **30** 1799
26. Bol A A, van Beek R and Meijerink A 2002 On the incorporation of trivalent rare earth ions in II–VI semiconductor nanocrystals *Chem. Mater.* **14** 1121
27. Chen W, Bovin J O, Joly A G, Wang S g, Su F and Li G 2004 Full-color emission from In_2S_3 and In_2S_3:Eu^{3+} nanoparticles *J. Phys. Chem. B* **108** 11927
28. Hu H and Zhang W 2006 Synthesis and properties of transition metals and rare-earth, metals doped ZnS nanoparticles *Opt. Mater.* **28** 536
29. Kenyon A J 2002 Recent developments in rare-earth doped materials for optoelectronics *Prog. Quantum Electron.* **26** 225
30. Sharma R K, Mudring A-V and Ghosh P 2017 Recent trends in binary and ternary rare-earth fluoride nanophosphors: How structural and physical properties influence optical behavior *J. Lumin.* **189** 44
31. Ghosh P, Sharma R K, Chouryal Y N and Mudring A-V 2017 Size of the rare-earth ions: a key factor in phase tuning and morphology control of binary and ternary rare-earth fluoride materials *RSC Adv.* **7** 33467
32. Ghosh P and Patra A 2005 Understanding the influence of nanoenvironment on luminescence of rare-earth ions *PRAMANA J. Phys.* **65** 901
33. Dahl J A, Maddux B L S and Hutchison J E 2007 Toward greener nanosynthesis *Chem. Rev.* **107** 2228
34. Sharma R K, Chouryal Y N, Chaudhari S, Saravanakumar J, Dey S R and Ghosh P 2017 Adsorption-driven catalytic and photocatalytic activity of phase tuned In_2S_3 nanocrystals synthesized via ionic liquids *ACS Appl. Mater. Interfaces* **9** 11651
35. Weingärtner H 2008 Understanding ionic liquids at the molecular level: facts, problems, and controversies *Angew. Chem. Int. Ed.* **47** 654
36. Marsh K N, Boxall J A and Lichtenthaler R 2004 Room temperature ionic liquids and their mixtures—a review *Fluid Phase Equilib.* **219** 93
37. Sharma R K, Nigam S, Chouryal Y N, Nema S, Bera S P, Bhargava Y and Ghosh P 2019 Eu-Doped BaF_2 nanoparticles for bioimaging applications *ACS Appl. Nano Mater.* **2** 927
38. Sharma R K, Chouryal Y N, Nigam S, Saravanakumar J, Barik S and Ghosh P 2018 Tuning the crystal phase and morphology of the photoluminescent indium sulphide nanocrystals and their adsorption-based catalytic and photocatalytic applications *ChemistrySelect* **3** 8171
39. Parnham E R, Slawin A M Z and Morris R E 2007 Ionothermal synthesis of β-NH_4AlF_4 and the determination by single crystal X-ray diffraction of its room temperature and low temperature phases *J. Solid State Chem.* **180** 49
40. Arco S D, Laxamana R T, Giron O D and Obliosca J M 2009 Synthesis of [RMIM] acetate halogen-free ionic liquids for use as greener solvents in Diels-Alder reaction *Philipp. J. Sci.* **138** 133